Fabrication, characterization and evaluation of *Manihot esculenta* starch based intelligent packaging films containing gum ghatti and black currant (*Ribes nigrum*) extract for freshness monitoring of beef meat

Changxing Jiang [a,*], Hongwu Yang [d], Tingting Liu [b,c,**], Qian Zhang [a], Yufei Zou [a], Siyu Wang [a]

[a] *School of Life Science and Food Engineering, Huaiyin Institute of Technology, Huai'an 223003, Jiangsu, PR China*
[b] *Affiliated Huai'an Hospital of Xuzhou Medical University and Huai'an Second People's Hospital, Huai'an 223002, Jiangsu, PR China*
[c] *The Second Affiliated Hospital and Yuying Children's Hospital of Wenzhou Medical University, Wenzhou, 325027, Zhejiang, PR China*
[d] *Xuzhou Medical University, Xuzhou 221004, Jiangsu, PR China*

ABSTRACT

In this study, active and intelligent films were fabricated using *M. esculenta* starch (MES), gum ghatti (GG) and *R. nigrum* extract (RNE) and their functionality, physicochemical properties and practical application were assessed. Incorporation of GG decreased water vapor permeability (WVP) (9.73 to 8.91×10^{-11} g m^{-1} s^{-1} Pa^{-1}), increased tensile strength (TS) (16.63 to 44.45 MPa) and elongation at break (EAB) (4.47 to 6.82%) of MES film. Incorporation of RNE decreased WVP (8.91 to 7.87×10^{-11} g m^{-1} s^{-1} Pa^{-1}) and TS (44.45 to 26.33 MPa) of MES-GG film. MES-GG-RNE films showed enhanced thermal stability, light barrier performance, excellent pH and ammonia sensitivities, strong antioxidant activity, and significant visible color change when monitoring beef freshness. Findings supported the application of this strategy in fabrication of MES-GG-RNE films for active and intelligent packaging. Further study on stability, sustainability and consumer acceptability of films is in progress.

1. Introduction

During storage and transportation of meat products, spoilage due to microbial infestation renders meat unacceptable for consumption and results in serious waste of food resources. Conventional approaches including cell culture, chemical assays and microbiological techniques are of great importance in safeguarding food quality. However, these methods are not appropriate for supermarkets due to the fact that they are frequently destructive, time-consuming and requires professional testing equipment (Liang et al., 2024). Therefore, there is an urgent need for developing a simple, non-invasive and consumer friendly method to assess the quality of meat and meat product (Elhadef et al., 2024). Recently, much effort has been made to active and intelligent films containing natural pH-dependent indicators, which can react with volatile basic nitrogen produced during microbial contamination and exhibit a noticeable shift in color determining the quality of packaged meat products.

As one of natural pigments, anthocyanins are easily soluble in water and found in a wide range of plants and fruits. Due to their pH sensitivity

of color shift and antioxidant and antimicrobial activities, anthocyanins are distinct from other pigments (Liang et al., 2024). The black currant (*R. nigrum*), known as cassis, belongs to the *Ribes* genus and widely cultivated for its edible fruits in Central and Northern Europe, New Zealand, China and Australia. Black currant is considered as an excellent supply of polyphenols with anthocyanins being the main type of phenolics (Paunović et al., 2017). In black currant fruits, four kinds of colorants were identified including delphinidin 3-O-rutinoside, cyanidin-3-O-glucoside, delphinidin 3-O-glucoside, and cyanidin-3-O-rutinoside, which made up 97% of the extractable anthocyanin content. The high content of anthocyanins in fruits of black currants were contributed to their significant biological effects, such as anti-microbial, anti-cancer, anti-mutagenic, anti-inflammatory and anti-hypertensive capacities (Paunović et al., 2017). Till now, anthocyanins derived from different berries, such as raspberries and strawberries, have been used to create pH-responsive intelligent films. Nevertheless, the use of black currant anthocyanins as a pH indicator in intelligent film production has not yet been extensively explored.

Biopolymers including chitosan, cellulose, gelatin and starch are

---

extensively applied to embed pH indicators in the smart films due to their non-toxic, ecologically beneficial and environmentally friendly characteristics. Cassava, belonging to the species of *M. esculenta* in the family Euphorbiaceae, is widely cultivated in tropical and subtropical regions. Cassava is rich in starches, which can be easily extracted and has a lot of advantages as a raw material for the biopolymer film production. Studies have indicated that cassava starch based films had desirable characteristics such as transparency, pliability, uniformity and easy biodegradation. Thus, cassava starch offers a viable alternative in development of economical, biodegradable films that are readily produced through a casting process with or without the use of plasticizers. However, for large-scale use, the water vapor permeability and mechanical strength of films made for food packaging still need to be enhanced (Gunathilake & Somendrika, 2024). Combined use of biopolymers has been proven to effectively improve tensile strength, water barrier property and thermal stability of composite films. Gum ghatti as an exudate gum of the tree belonging to the family of the *Anogeissus Indifolia* growing in India, shows outstanding properties such as nontoxicity, gelling characteristics and high solubility and potentially be useful in manufacture of films due to its component glycoprotein. However, there is no report on using gum ghatti in fabrication of intelligent packaging films compared with some other plant-derived gums like tara gum, basil seed gum and locust bean gum. Therefore, we report here a new active and intelligent film that was developed by blending black currant fruit anthocyanin with *M. esculenta* starch and gum ghatti. The film was characterized by using Fourier transform infrared spectroscopy, scanning electron microscopy and X-ray diffraction spectra, followed by tests of color, moisture content, water vapor permeability, light transmittance, thermal stability, mechanical property, antioxidant capacity *in vitro*, pH and ammonia sensitivities. Finally, the potential application of composite films in beef meat was studied.

2. Materials and methods

2.1. Materials and reagents

The fresh fruits of *R. nigrum* were purchased on May 2023 from Huaian Huilong fruit wholesale market in Huaian, China. The fruits were moved to the laboratory, cleaned with distilled water, and kept at −80 °C until they were needed. Gum ghatti and cassava (*M. esculenta*) starch was obtained from Wangwang Biotechnology Co., Ltd. (Shanghai, China). DPPH was provided by Huaian Kaitong Chemical Reagent Co. LTD (Huaian, China). The other reagents were all analytical grade.

2.2. Extraction of anthocyanins

Extraction of anthocyanins was performed using the methodology recommended by Wang, Du, et al. (2019) with some adjustments. Briefly, 100 g raw material was homogenized and steeped in 1 L of ethanol at a concentration of 80% containing 1% HCl to improve the stability of the anthocyanins. The extraction was done twice at 4 °C for 24 h to extract anthocyanins completely. The resulting solution was put on an AB-8 macroporous resin column, continuously eluted with 80% ethanol solution containing 1% HCl (*v/v*) and followed by a 15-min centrifugation at 4000 rpm and 4 °C. The obtained supernatant was concentrated using a vacuum rotatory evaporator at 30 °C. The total anthocyanin content in the fruit and black currant extraction (RNE) solution was detected by using pH differential assay. The resulting RNE solution was kept in the dark until it was needed again.

2.3. pH-sensitivity test of RNE

The pH-sensitivity of RNE was assessed using the method of Zhang, Liu, Qian, et al. (2019) with few revisions. In short, various buffer solutions (10 mL) with pH of 2–13 were mixed with 0.4 mL of RNE solution, vortexed for 1 min, and kept in darkness at 4 °C. After a storage time of 10 min, color of the RNE solution was obtained using a camera phone. The absorption spectra of RNE were gained by a UV-3600 spectrophotometer at wavelengths spanning from 250 to 700 nm.

2.4. Development of films

Films were developed using previously published methods with slight modifications (Cao et al., 2023). Briefly, 4.5 g MES was added to 150 mL distilled water and gelatinized in boiling water for 30 min. Then, the gelatinized MES paste was mixed with 1.35 g of GG and 1.25 g of glycerol and kept heated for 1 h. After cooling to 40 °C, the mixed blend was added to various amounts of RNE (0, 1.5 mL/g, 3 mL/g and 4.5 mL/g, on the basis of MES), poured into a 24 cm × 24 cm mould, which was put in the water bath, adjusted horizontal using a spirit-level and dried at 30 °C for 48 h. In this way, four MES/GG/RNE based films including the MES, MES-GG, MES-GG-RNE-I, MES-GG-RNE-II and MES-GG-RNE-III films were produced. Prior to analysis, films were kept at 50% RH and 20 °C for 2 days.

2.5. Structural characterization of the films

The structural characterization of MES, MES-GG and MES-GG-RNE films was performed based on the methods of Cao et al. (2023) with some modifications. Briefly, Fourier transform infrared (FTIR) spectrum of films was acquired on a Nicolet 5700 FTIR spectrometer (Thermo Nicolet 5700, Thermo Nicolet Corporation, Wisconsin, USA) equipped with attenuated total reflectance mode in the frequency range of 400–4000 cm^{-1}. Cross-sectional images of film were captured at 1500× by a scanning electron microscope (Phenom Pro, Phenom World, Netherlands). Film's X-ray diffraction (XRD) patterns were obtained using a D8 Advance diffractometer (Bruker AXS GmbH, Karlsruhe, Germany) with Ni-filtered Cu Kα radiation.

2.6. Determination of the physical properties of the films

2.6.1. Thickness and color

Thickness of films was assessed using a screw micrometer (WD, Wenzhou Weidu Electronic Co., Ltd., Zhejiang, China) with accuracy of 0.001 mm (Zhang, Liu, Qian, et al., 2019). Color parameters (*L*, *a* and *b*) of films were recorded by a CR-10 colourimeter (Konica Minolta, JPN). The total color difference (Δ*E*) of films was calculated as follows:

$$\Delta E = \sqrt{\Delta L^2 + \Delta a^2 + \Delta b^2} \tag{1}$$

where Δ*L*, Δ*a* and Δ*b* were difference between each color value of active and control films.

2.6.2. Moisture content (MC) and water vapor permeability (WVP)

MC was determined using the conventional oven drying method. Film samples (5 cm × 5 cm) were dried at 105 °C until constant weight and MC of films was calculated based on weight loss of samples. The WVP of films was determined using the gravimetric method. 6 cm × 6 cm of film specimens were attached on a centrifuge cup filled with 40 g of dry silica gel and kept at 20 °C in a desiccator with 100% relative humidity. The daily weight change of centrifuge cup was recorded for 5 days at 20 °C. The WVP (g m^{-1} s^{-1} Pa^{-1}) of films was computed following the equation below:

$$WVP = \frac{W \times x}{t \times A \times \Delta P} \tag{2}$$

where *W* stands for the change in silica gel weight (g), *x* for film thickness (m), *t* for time (s), *A* for the film sample's permeation area (m^2), and Δ*P* for saturated vapor pressure at 20 °C.

2.6.3. Light transmittance and opacity

Light transmittance of films was tested on a UV-3600 ultraviolet-

visible spectrophotometer (Shimadzu, Japan) in ultraviolet visible region varied from 200 to 700 nm. Based on the absorbance of films at 600 nm, The opacity of films was computed following the equation below:

$$Opacity = \frac{A_{600}}{x} \tag{3}$$

where x and A_{600} are the thickness (mm) and absorbance of film at 600 nm, respectively.

2.6.4. Thermal stability

Thermal stability was analyzed by a Netzsch TG 209 instrument (Netzsch-Gerätebau GmbH, Selb, Germany) at 50–800 °C. 2 mg of film specimen was heated at a heating rate of 10 °C/min and under a nitrogen flow of 20 mL/min (Wang et al., 2018).

2.6.5. Mechanical property

Mechanical property of films was evaluated by testing the tensile strength (TS) and elongation at break (EAB) using a CT3 Brookfield texture analyzer. The experiment was run with a 50 mm gauge length, a 50 RH%, and a 20 mm/min stretching speed at 25 °C. TS and EAB were computed following the equation below (Wang, Yong, et al., 2019):

$$TS = \frac{F}{L \times S} \tag{4}$$

$$EAB(\%) = \frac{H - H_0}{H_0} \times 100 \tag{5}$$

where F stands for the maximum axial tensile force (N), S for the film thickness (mm), and L, H_0 and H for the width, initial and final lengths (mm) of films, respectively.

2.6.6. Water contact angle

A contact angle meter (Theta Flex, Biolin Scientific, Sweden) was used to evaluate the water contact angle of the film samples. 4 μL of deionized water was dropped on the surface of film samples (2 × 2 cm). The angle was recorded and repeated three times (Kaewprachu et al., 2024).

2.7. Antioxidant capacity in vitro

2.7.1. DPPH radical assay

Film samples (4, 8, 12, 16, and 20 mg) were added into 4 mL of DPPH ethanol solution with a concentration of 100 μM and kept in darkness at 4 °C for 1 h. The absorbance of the reaction solution was measured at 517 nm. The scavenging activity of films on DPPH radical was computed using the formula below:

$$DPPH \ radical \ scavenging \ activity \ (\%) = \frac{A_0 - A_1}{A_0} \times 100 \tag{6}$$

where A_0 and A_1 are the absorbance of DPPH solution without and with film samples, respectively.

2.7.2. ABTS radical assay

The ABTS stock solution was prepared by mixing 1:1 of ABTS (7 mM) and potassium persulfate (2.45 mM) solutions, which was followed by reaction in the dark at 20 °C for 12 h. 4, 8, 12, 16 and 20 mg of film sample was added to 4 mL of the ABTS solution, of which the absorbance was diluted to about 0.7 at 734 nm with absolute ethanol and kept in darkness for 1 h at 4 ∘C. Thereafter, the absorbance of reacted solution was measured at 734 nm using a UV-3600 ultraviolet-visible spectrophotometer (Shimadzu, Japan). The scavenging percentage on ABTS radical was computed using the formula below:

$$ABTS \ radical \ scavenging \ activity \ (\%) = \frac{A_0 - A_1}{A_0} \times 100 \tag{7}$$

where A_0 and A_1 are the mixture of absolute ethanol and ABTS, and sample and ABTS solution, respectively.

2.8. pH- and ammonia-sensitivity

The pH sensitivity was assessed by recording color changes of samples (2 cm × 2 cm), which was immersed in various buffers (pH 2–13) for 1 min using a digital camera. The ammonia sensitivity was evaluated by recording color changes of samples (2 cm × 2 cm) every 5 min, which was immersed in 0.1 mol/L ammonia solution.

2.9. Application of films

A transparent plastic box was filled with 80 g of fresh beef meat, sealed with lid, which inner surface was pasted by 3 cm × 1 cm of film samples, and kept for 48 h at room temperature. The change in color of films was recorded every 24 h. The total volatile basic nitrogen (TVB-N) of the beef was evaluated at the same time according to the Chinese standard GB 5009.237–2016. Briefly, 4 g of sample was homogenized in 30 mL of deionized water and filtrated. The filtrate (5 mL) was added to 1% MgO suspension (5 mL), mixed well and distilled in a Kjeldahl apparatus. The distillated was collected into a flask containing methylene blue indicator and 2% boric acid solution (10 mL) and titrated with 0.01 M of HCl solution. The TVB-N levels were calculated based on the HCl amount consumed with a unit of mg/100 g.

2.10. Statistical analysis

All data are expressed as mean ± standard deviation (SD). Duncan's test and one-way analysis of variance (ANOVA) were performed by GraphPad Prism 8 software. In Section 3, different letters in the same column indicate significant differences ($p < 0.05$).

3. Results

3.1. Anthocyanin content and pH sensitivity

The content of anthocyanins in black currant fruits was tested using pH differential method. Our analysis's findings demonstrated that the fresh fruit had a high content of anthocyanin (3.58 mg/g), indicating its potential in using as pH indicator of intelligent film. Slimestad and Solheim (2002) revealed that the delphinidin and cyanidin were the main anthocyanins in black currant fruits, making up > 97% of total anthocyanins. Anthocyanin can present different colors due to alteration of the structures as the environment was shifted from acidic to alkaline ones (Halász and Csóka, 2018). As showed in Fig. 1, RNE presented different color at various pHs. As pH was 2–13, color of RNE turned from red to brown. In a high acid environment (pH 2–3), RNE color showed signal red, resulted from the formation of flavylium cations. It became light pink when the pH was 5 and 6. In neutral environment (pH 7), the color of RNE was deep pink due to the formation of carbinol bases. As pH was changed from 8 to 11, the RNE color was changed from blue to green to yellow, resulting from formation of quinoidal anhydrobase. In a strong alkaline environment (pH 12 and 13), the color of RNE was signal brown, attributed from the degradation of anthocyanins in alkaline environment (Merz et al., 2020). The findings demonstrated colors of RNE were sensitive to pH changes due to structural changes of functional groups in the anthocyanin molecules. Many studies have focused on color sensitivity to pH of anthocyanins from various plants such as blood orange (Zhao et al., 2023), jambolan (Merz et al., 2020) and mulberry pomace (Zhang, Chi, et al., 2023). To further investigate the relationship between the pH and the optical characteristics of anthocyanins, UV–visible spectra were obtained for RNE at different pHs. As showed in Fig. 1, the RNE solution at pH shifted from 2 to 13 showed obvious absorption in the UV region of 270–330 nm, which was in
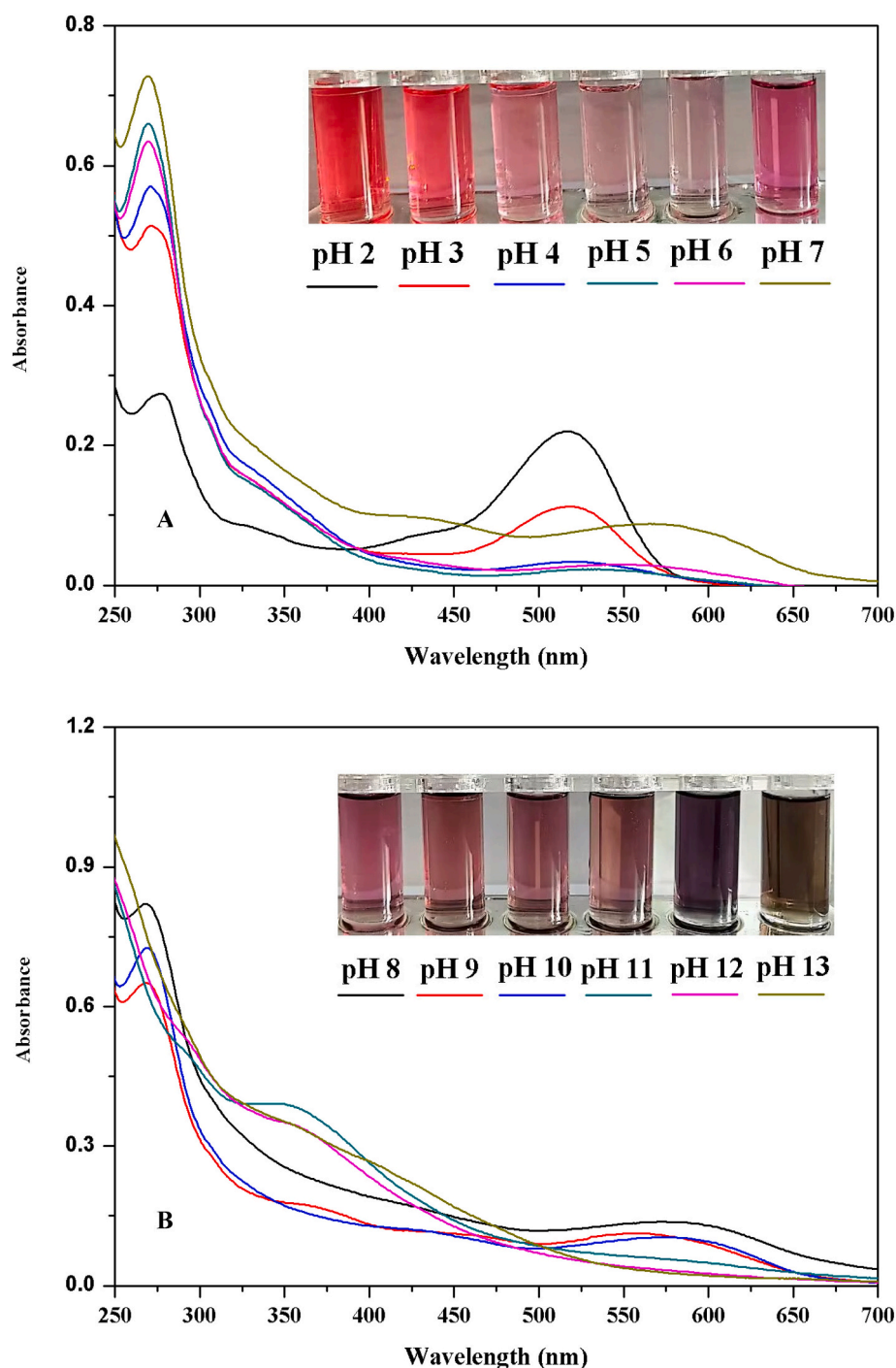
Fig. 1. Color response to pH and ultraviolet-visible spectra of RNE.

accordance with our previous study on pH sensitivity of *Oxalis triangularis* extract (Jiang, Liu, Wang, et al., 2023). The greatest absorption peak was observed in 400–700 nm at pH 2–6, suggesting the flavylium cation (AH$^+$), which was responsible for the red color was the major form of anthocyanins presented in the acidic solution. When pH of the RNE solution was at 7–13, the strongest peak was weakened and shifted to 580 nm. Similar findings were made in an earlier investigation (Yong, Wang, et al., 2019). These findings revealed that the black currant extract had great potential in fabrication of pH-sensitive freshness-indicating labels.

3.2. Structural characterization

FTIR spectra of pure starch film (MES), MES-GG film, and MES-GG-RNE-I, MES-GG-RNE-II and MES-GG-RNE-III films (containing 1.5 mL/g, 3 mL/g and 4.5 mL/g of RNE, on the basis of MES) in the wavenumber 400–4000 cm^{-1} are presented in Fig. 2A. The peaks at 3280 and 2917 cm^{-1} might be resulted from the stretching vibration of O—H and C—H, respectively. Peaks in the 1200 cm^{-1} to 1350 cm^{-1} range were contributed to C—O stretching vibrations in the starch mixture (Ranjbar et al., 2023). Peaks in the region of 950 cm^{-1} to 1190 cm^{-1} were linked to the vibrational modes and connections of the C–O–C bonds (Ranjbar et al., 2023). Moreover, the peak in the 650 cm^{-1} to 930 cm^{-1} region
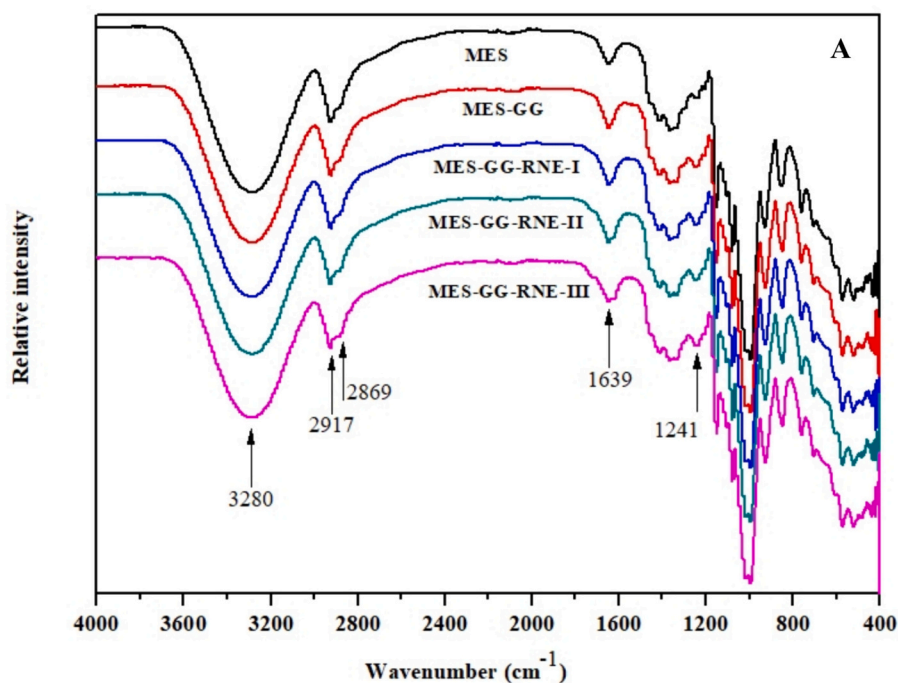
Fig. 2. Patterns of FTIR (A), SEM (B) and XRD (C) for the MES, MES-GG and MES-GG-RNE films.

was thought due to the presence of C≡C and C—H bonds (Li et al., 2014). The peaks at 3280 cm^{-1} and 2917 cm^{-1} were attributed to –OH and C—H stretching vibrations of GG, respectively (Kaith et al., 2014). Peaks at 1639 cm^{-1} and 1241 cm^{-1} were resulted from skeletal vibration of the aromatic and heterocyclic rings in cyanidin-3-glucoside (Zhao et al., 2023). No noticeable difference or no peak in was observed in FTIR spectrum of the MES-GG or MES-GG-RNE film, indicting that no new covalent bonds came into being during fabrication of films. The bonding between RNE and the MES/GG blend can be attributed to physical interacting strength including van der Waals and hydrogen forces. Similarly phenomenon were observed in chitosan/gum arabic and potato starch based films, for which no new peaks appeared in FTIR spectra after blending with blood orange and *Clitoria ternatea* flower anthocyanins (Jiang, Zhang, Cao, & Jiang, 2023).

The morphologies and interface compatibility between glycerol, MES, GG and RNE of the composite films were assessed through observing their cross-sections, as depicted in Fig. 2B. From the diagram it could be observed that the MES film showed an irregular surface with varying size white spots and bubbles. The white spots might be due to the undissolved MES granules; while the bubbles were attributed from high temperature and less amount of glycerol used for fabrication of film. The MES-GG film showed a homogeneous mass of the cross-section profiles, indicating GG was evenly distributed in the MES film. This result was due to the fact that both MES and GG had the same polarity and created strong intermolecular interactions. The MES-GG film showed different cross-section morphology after introduction of different amount of RNE. When the RNE content was at a low level (1.5 mL/g), the cross-section of the MES-GG-RNE-I film showed a compact phase that did not differ from that of the MES-GG film, indicating low level of RNE content did not disturb the intermolecular interaction between MES and GG. When the RNE content was 3 mL/g, the cross-section of the MES-GG-RNE-II film was also comparatively flat and dense. The reason for this was partly the plasticizing role of the RNE added to the composite films, which opened the entanglement structure between the MES molecular chains and strengthened the network structure formed between the MES matrix and glycerol. In addition, the dense and

smooth cross-section of the MES-GG-RNE-II film were attributed to the fact that the hydroxyl group in RNE could form new hydrogen bonds with that of the MES, reduce the arrangement of hydrogen bonds between starch and glycerol, therefore changing the intermolecular entanglements in the MES-GG film. As the content of RNE was 4.5 mL/g, the cross-section of the MES-GG-RNE-III film began to become rough with some obvious concave faces, indicating the uniformity of the film cross-section was seriously damaged. According to our findings, the excess RNE added to the film matrix could destroy the cross-section's compact structure, which would impair the composite films' mechanical and barrier qualities (Jiang, Zhang, & Jiang, 2023).

Crystallinity is an important criterion for characterizing composite film materials because of its close relationship with the properties and structures of films (Zhang, Yang, et al., 2023). X-ray diffraction was used to observe effects of film components on crystallinities and structures of film solid system. The XRD pattern of the MES, MES-GG and MES-GG-RNE films is shown in Fig. 2C. Starches, existing as granules with different shapes and dimensions, can be categorized into three kinds such as A-type (big), B-type (middle) and C-type (small). MES showed characteristics of A-type starches with distinct peaks at 15°, 17°, 18° and 23° (Ji et al., 2022). Nevertheless, some MES diffraction peaks vanished from the film after gelatinization, which was explained by the starch granule crystalline was destroyed by mechanical stirring and heating during gelatinizing process. The MES-GG film presented a broad and weak peak at $2\theta = 20$, which may have been caused by the GG molecules adhering to the starch surface and breaking down the crystalline domains of the biopolymer. The MES-GG-RNE films had a similar position of diffraction peak with the MES-GG film, indicating incorporation of GG and low-level RNE did not change the crystal structure of MES film. The diffraction peak intensity of the MES-GG-RNE-II and MES-GG-RNE-III films with higher RNE contents (3 and 4.5 mL/g, respectively) was significantly lower than that of the MES or MES-GG film. Our results suggested that high level of RNE addition somewhat decreased the crystallinity of the MES-GG films. The reduced crystalline degree of the MES-GG-RNE films might be attributed to strong H-bond interaction newly formed between RNE and MES/GG. The results agreed with the
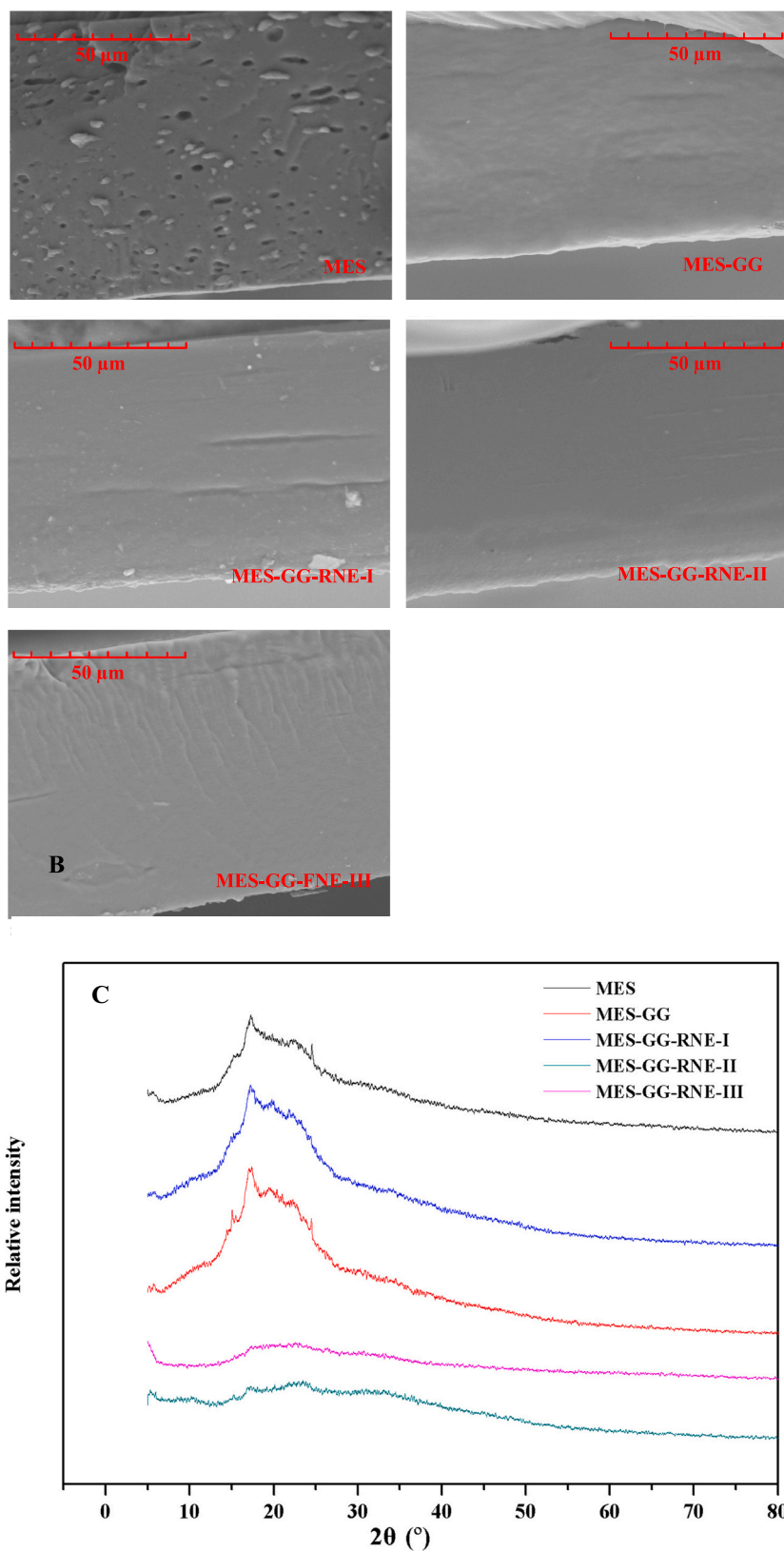
Fig. 2. (*continued*).

finding that the MES-GG-RNE-III film had a rough cross-section (Fig. 2B). Inconsistent results were given by Li, Feng, et al. (2024) who reported incorporation of bilberry anthocyanins increased the intensities of the film peaks located at $2\theta = 20.8$ due to the chain rearrangement of sodium alginate or gum ghattin polymer and the formation of an additional intramolecular H bond interaction of the bilberry anthocyanins with film substrates. Our findings showed a possible relationship between the crystallinity degree of films and the

composition and content of polyphenol-rich extracts.

3.3. Physical properties of films

3.3.1. Color and thickness

Food packaging color is one of the most important factors that influenced the consumer choice. As illustrated in Table 1, MES and MES-GG films were color less and transparent, while MES-GG-RNE films showed purple colors. With the addition amount was increased, the purple color of MES-GG-RNE films deepened. Similar results were found as the chitosan films were added with the Ag and nickel oxide nanoparticles, respectively (Mouzahim et al., 2023). Every color has a unique set of ΔL, Δa, and Δb values. For instance, ΔL is for luminance, which ranges from absolute transparency or whiteness to complete opacity or blackness; Δa reflects red or green, and Δb denotes blue or yellow. As depicted in Table 1, ΔL value of -2.52 suggested the MES-GG film was darker than the MES film. Δa and ΔE of MES-GG film were higher than those of the MES film ($p < 0.05$). The increased Δa and decreased Δb suggested the color of MES-GG film was red and blue, which was resulted from the incorporation of GG with a light-orange color. The MES-GG-RNE films showed significantly lower ΔL and Δb but higher Δa and ΔE than the MES-GG film ($p < 0.05$). The lower Δb and higher Δa for the MES-GG-RNE films indicated the films' tendency to red and blue color. The MES-GG-RNE-III film showed significantly higher values of Δa and ΔE but significantly lower values of ΔL and Δb than the MES-GG-RNE-II film. The result suggested colors of the MES-GG-RNE films were significantly influenced by incorporation content of RNE.

As present in Table 2, the MES film had a thickness of 0.082 mm, while the MES-GG film thickness was 0.075 mm. The thickness of the MES and MES-GG films was significantly different. After introducing RNE, the thickness of the MES-GG film became markedly increased ($p < 0.05$). The MES-GG-RNE-II and MES-GG-RNE-III films showed a greater thickness ($p < 0.05$) when compared with the MES-GG-RNE-I film. The increase in thickness of the MES-GG-RNE-II and MES-GG-RNE-III films was due to a relatively high content of RNE in film matrix, which could prolong the spatial distance of film substrates destroy the original crystal structure of film matrix.

3.3.2. MC and WVP

Within a packaged product, food packaging films should maintain some level of certain moisture which are transferred from relatively high humid environment (Yong, Wang, et al., 2019). Table 2 shows the change in the MC with various concentrations of RNE and GG in films. The MES film had the maximum MC of 16.7%, which was resulted from that MES was highly hygroscopic in nature and there were strong hydrogen bonds generated between water and MES (Yong, Liu, et al., 2019). Incorporation of GG significantly reduced MC of the MES film ($p < 0.05$). The MC of MES-GG-RNE films was markedly decreased ($p < 0.05$) when the RNE addition amount was raised. The lowest MC

(12.3%) was found when the amount of RNE was 4.5 mL/g. The decreased MC of the MES-GG-RNE films was resulted from the decreased availability of hydrophilic groups in MES, caused by strong hydrogen bond interactions newly formed between hydroxyl group in RNE and MES.

WVP is vitally important for food packaging films, for which low WVP that represent excellent water vapor barrier properties is required. As shown in Table 2, the MES film had a relatively higher WVP (9.73×10^{-11} g m^{-1} s^{-1} Pa^{-1}), manifesting a relatively weak water vapor barrier property. This was attributed to that MES film was primarily composed of hydrophilic polysaccharides, which could break the ordered arrangement of polysaccharide chains and disturb the film structure by forming hydrogen bonds with water molecules through their polar groups (-OH and -COOH) on the chain. The addition of GG and RNE could significantly decrease WVP of MES film. A probable explanation for it was that the incorporation GG and RNE resulted in a dense network microstructure that improved the properties of the water barrier by lengthening the diffusion path of water molecules and so limiting their diffusion. Similar findings were reported by Zhou et al. (2021) who found incorporation of mulberry pomace extracts significantly reduced the WVP of the konjac glucomannan films. WVP of the MES-GG-RNE films decreased significantly with increase of RNE addition amount. The MES-GG-RNE-III film with the highest addition amount of 4.5 mL/g showed the minimum WVP (7.87×10^{-11} g m^{-1} s^{-1} Pa^{-1}), indicating an excellent water vapor barrier activity. The excellent water vapor barrier of the MES-GG-RNE films was beneficial for most food packaging applications because it could prevent changes in food texture and suppress microbiological development.

3.3.3. Light transmittance

The opacity of packaging film is important factors affecting their practical applications. A transparent film helps purchasers observe contents and assess qualities of foods directly. On the other hand, it can also pass light, causing foods vulnerable to oxidation and corruption reactions. As displayed in Fig. 3A, the MES film had the highest ultraviolet-visible light transmittances due to lacking light absorption groups. When RNE content in the film was increased, the films showed a significant decrease in light transmittance. Notably, the MES-GG-RNE films exhibited markedly UV rejection capacity at 200 nm to 300 nm, as RNE content was increased (1.5 to 4.5 mL/g). The increased UV barrier ability was because of the abundant light absorption groups in RNE. The result was similar to that of Wang, Cao, et al. (2023), who confirmed incorporation of black chokeberry extract markedly enhanced the UV rejection ability of arrowhead starch/κ-carrageenan composite films. The opacity value of the film samples is presented in Table 2. The MES film showed an opacity of 3.39 ± 0.10 mm^{-1}, indicating its good light-blocking properties. The opacity of MES-GG film (4.95 ± 0.09 mm^{-1}) was significantly higher than that of the MES film ($p < 0.05$), suggesting incorporation of GG could significantly improve the light-blocking properties of films. The MES-GG-RNE films showed an opacity range of 2.81–3.70 mm^{-1}, which had no significant difference with that of the MES film and was significantly higher than that of the composite films fabricated using cassava starch, κ-carrageenan and black nightshade extracts (0.85–3.16 mm^{-1}) (Cao et al., 2023). Our study results indicated that the MES-GG-RNE film had excellent light transmittance capacity and could be applied in an active food packaging.

3.3.4. Thermal stability

As shown in Fig. 3B and Fig. 3C, three stages of weight loss were shown on the TGA curve for each film. The first stage was at 117–159 °C, showing a weight loss of 6.01–7.19%, which was resulted from the evaporation of absorbed or H-bonding water in the films. The second stage (205–233 °C) with weight loss of 10.12–12.31% was associated with the glycerol decomposition. The third stage was at 259–346 °C, related to the removal of polyhydroxyl groups from starch, as well as the depolymerization and disintegration of the film matrix. As the

Table 1
Color values of the MES, MES-GG and MES-GG-RNE films.

Films	Color	ΔL	Δa	Δb	ΔE
MES					
MES-GG		-2.52 ± 0.42 [a]	3.48 ± 0.25 [c]	-1.05 ± 0.17 [a]	4.44 ± 0.01 [d]
MES-GG-RNE-I		-6.03 ± 0.23 [b]	8.96 ± 0.39 [b]	-2.51 ± 0.08 [a]	10.73 ± 0.95 [c]
MES-GG-RNE-II		-8.15 ± 1.65 [b]	11.28 ± 1.22 [ab]	-3.07 ± 0.39 [ab]	14.26 ± 1.99 [b]
MES-GG-RNE-III		-10.92 ± 0.49 [c]	14.04 ± 3.18 [a]	-4.72 ± 0.03 [b]	19.97 ± 0.55 [a]

MES film with L (87.32), a (-0.46) and b (-2.21) is used as controls.

Table 2
Physicochemical properties of the MES, MES-GG and MES-GG-RNE films.

Films	Thickness (mm)	MC (%)	Opacity (mm^{-1})	WCA (º)	WVP (10^{-11} g m^{-1} s^{-1} Pa^{-1})	Mechanical properties	
						TS (MPa)	EAB (%)
MES	0.082 ± 0.001 [b]	16.7 ± 0.2 [a]	3.39 ± 0.10 [bc]	83.83 ± 3.38 [a]	9.73 ± 0.31 [a]	16.63 ± 0.86 [d]	4.47 ± 0.37 [c]
MES-GG	0.075 ± 0.003 [c]	14.5 ± 0.4 [b]	4.95 ± 0.09 [a]	67.68 ± 3.96 [b]	8.91 ± 0.38 [b]	44.45 ± 0.88 [a]	6.82 ± 0.38 [b]
MES-GG-RNE-I	0.082 ± 0.002 [b]	14.2 ± 0.3 [c]	3.70 ± 0.12 [b]	61.83 ± 1.81 [bc]	8.41 ± 0.16 [bc]	36.06 ± 1.48 [b]	6.47 ± 0.09 [b]
MES-GG-RNE-II	0.088 ± 0.004 [a]	12.7 ± 0.2 [d]	2.81 ± 0.07 [c]	56.23 ± 2.23 [c]	8.06 ± 0.23 [c]	38.88 ± 2.19 [b]	13.78 ± 0.80 [a]
MES-GG-RNE-III	0.088 ± 0.002 [a]	12.3 ± 0.1 [d]	3.32 ± 0.05 [bc]	84.00 ± 1.16 [a]	7.87 ± 0.36 [c]	26.33 ± 1.3.3 [c]	11.91 ± 0.52 [a]

temperature arrived at 800 °C, the residual weight ratios for the MES, MES-GG and three MES-GG-RNE films were 8.95%, 14.26%, 15.77%, 16.84% and 13.33%, respectively. Obviously, at 800 °C, MES-GG and MES-GG-RNE films had larger percentage of residual mass than MES film, suggesting the temperature stability of MES-GG and MES-GG-RNE films was enhanged after the addition of GG or RNE (Fig. 3B). Prietto et al. found that the film without anthocyanins was degraded completely (Prietto et al., 2017). In our study, RNE slightly enhancing thermal stability of MES-GG film was partly due to intermolecular interactions formed among MES, GG and RNE (Zhang, Liu, Yong, et al., 2019). Furthermore, GG and RNE did not alter the values of MC$_{100}$ and T$_{90}$ of the MES-GG-RNE films, indicating MES-GG-RNE films were stable when the test temperature was <100 °C. The DTG peak maximum of the MES film was 331 °C, which was higher than that of the MES-GG or MES-GG-RNE films (285–296 °C) (Fig. 3C). The findings suggested that the addition of GG and FRE could modify the MES film's thermal characteristics as well as the way moisture interacts with the starch matrix.

3.3.5. Mechanical property

The mechanical property of packaging films, usually assessed as TS and EAB, are the behavior of films in response to an applied force. It is important for a packaging film to possess sufficient mechanical index in preventing packaging failure during food distribution. TS and EAB of the MES, MES-GG, and MES-GG-RNE films are present in Table 2. TS and EAB of MES film was 16.63 MPa and 4.47%, respectively. And those of MES-GG film were 44.45 MPa and 6.82%, respectively, which was higher than those of MES film. The enhanced TS of MES-GG film was due to the strong hydrogen interaction which enhanced the cohesion of the cross-linked network, improving the strength of films. Many factors, such as nature of the molecule themselves, electrostatic and hydrogen bonding interactions had certain effect on mechanical property of films. Hydrogen interaction could promote mechanical properties of films theoretically. While the electrostatic interaction might disturb the ordered arrangement structure of MES or GG molecules and decrease structural cohesion and intermolecular force between the MES and GG chains. Furthermore, an excess content of anthocyanins in film matrix could hinder the movement and rotation of the MES and GG molecule chains, reducing the formation of intermolecular hydrogen bond and causing a decrease in the mechanical properties (Jiang et al., 2022).

3.3.6. Water contact angle

WCA is an important indicator of the films surface wettability. The WCA of a film surface indicates a hydrophilic (contact angle < 90º) or hydrophobic (contact angle > 90º) nature (Kaewprachu et al., 2024). As shown in Table 2, all film samples tested showed a WAC range of 56.23–84.00º, indicating their hydrophilic character. The MES film had a high WAC of 83.83º, indicating that the film had poor wettability. The WCA of MES film was decreased to 67.68º (MES-GG film) after incorporation of GG, representing a reduction in surface hydrophobicity of composite films. The addition of RNE also significantly influenced the WCA of composite films. As the addition amount of RNE was increased from 1.5 mL/g to 3 mL/g, WCA of films was decreased from 61.83 ± 1.81° (MES-GG-RNE-I film) to 56.23 ± 2.23° (MES-GG-RNE-II film). The decreased WCA of composite films were attributed to a large

number of hydrophilic hydroxyl groups of anthocyanins in RNE. When the addition amount of RNE was increased from 3 mL/g to 4.5 mL/g, WCA was increased to 84.00 ± 1.16° (MES-GG-RNE-III film) due to the aggregation of RNE, which could increase the roughness of film surface and promotes the surface hydrophobicity of the film. Liu et al. (2019) also believed that WCA of the composite film was related to the surface hydrophobicity and roughness of films.

3.4. Antioxidant activities in vitro of the films

Extremely reactive chemicals known as free radicals have the potential to oxidize different food ingredients and cause spoiling. By scavenging these free radicals and shielding food from oxidative stress, antioxidants safeguard food qualities and lengthen its storage times. The antioxidant capacities of the MES-GG and MES-GG-RNE films were assessed by determining eliminating rates on the free radical of DPPH and ABTS. As depicted in Fig. 4A and Fig. 4B, the MES-GG and MES-GG-RNE-I films showed low scavenging rates on the radicals of DPPH and ABTS. The radical eliminating rates of the MES-GG and MES-GG-RNE-I films were kept below 30% as the addition amount of film was increased from 1 to 5 mg/mL. The MES-GG-RNE-II and MES-GG-RNE-III films showed dose-dependent antioxidant activity. When the addition amount of films was 1 mg/mL, the eliminating rate on DPPH radical was 26.3% and 30.5% for the MES-GG-RNE-II and MES-GG-RNE-III film, respectively. While the ABTS radical scavenging rates were 22.1% and 38.9% for the MES-GG-RNE-II and MES-GG-RNE-III film, respectively. When the addition amount of films was 5 mg/mL, the eliminating rates on DPPH radicals were significantly increased to 47.8 and 76.3% for the MES-GG-RNE-II and MES-GG-RNE-III film, respectively. While the ABTS radical scavenging rate for the MES-GG-RNE-II and MES-GG-RNE-III film was significantly increased to 46.1% and 60.8%, respectively. At the same film addition amounts, the eliminating rates on DPPH or ABTS were MES-GG-RNE-I < MES-GG-RNE-II < MES-GG-RNE-III. The improvement in antioxidant activities of the MES-GG-RNE films might be resulted from anthocyanins of RNE, which can trap free radicals and terminate its chain reactions. Several studies have demonstrated that natural pigments considerably increased the antioxidant activity of biopolymer films (Guo et al., 2024; Li, Zhang, et al., 2024 Wang, Yong, et al., 2019). Our study results indicated that the MES-GG-RNE film had excellent capacity of trapping free radicals and could be applied in an active food packaging.

3.5. pH- and ammonia-sensitivities

Colors of the food packaging film play an important visual role and directly influence consumer perception. The MES-GG film was transparent and colorless when exposed to different pH buffers (data not shown). The color of the MES-GG-RNE films response to various buffer solutions are given in Fig. 4C. It could be found these MES-GG-RNE films were scarlet when the pH was 2. When pH arrived at 6, the color of MES-GG-RNE films was faded little by little and turned into roseate and light pink-brown. When pH was altered from 7 to 11, the color was changed to sea green. The findings suggested RNE incorporation could markedly increase pH-sensitivity of the MES-GG film, which agreed with the
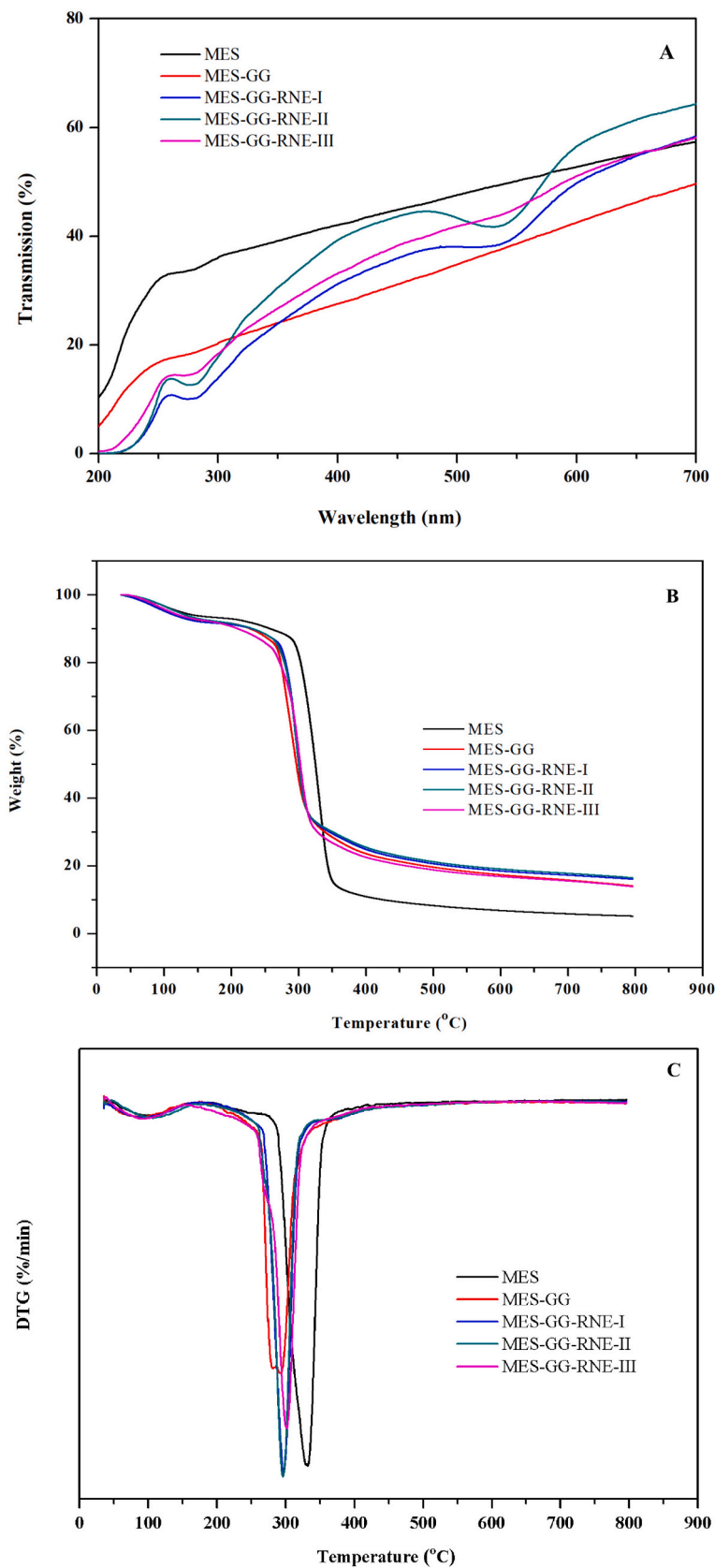
Fig. 3. Curves of UV–vis light transmittance (A) and TGA (B) and DTG (C) of the MES, MES-GG and MES-GG-RNE films.
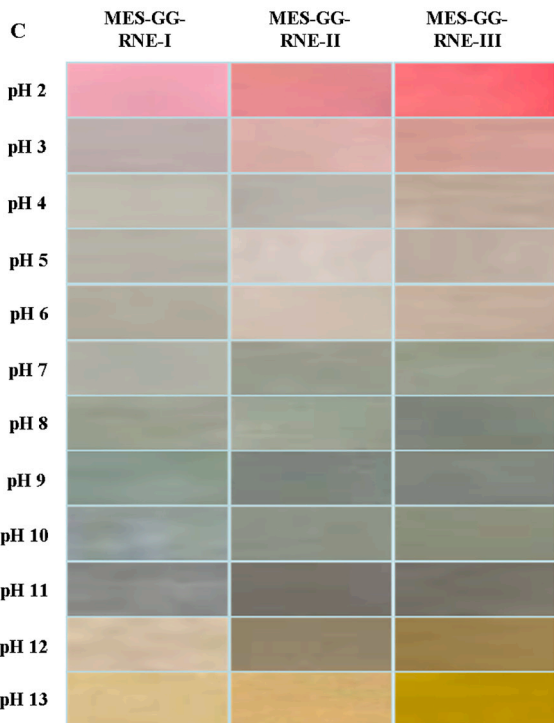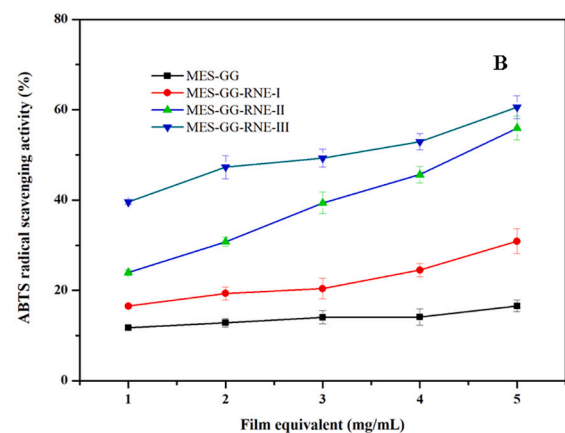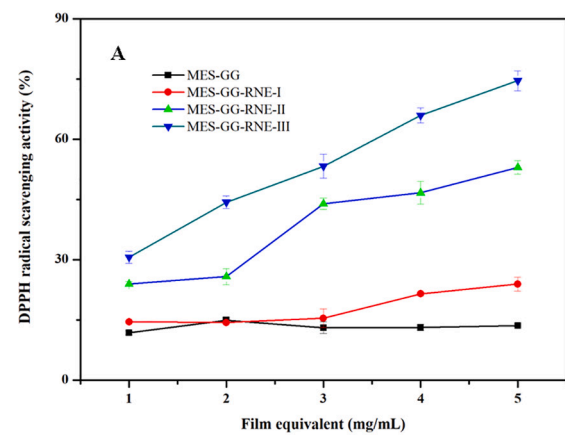
Fig. 4. DPPH (A) and ABTS (B) free radical scavenging activities and color pH response (C) of films.

results of color pH-response of RNE (Fig. 1). When the pH was raised to 12–13, the MES-GG-RNE films turned yellow. The yellow color became deepened with the RNE addition amount was increased. The color change of the MES-GG-RNE films was due to the structural transformation of anthocyanin when the solution was changed from acidic environment to alkaline ones. Some recent literature has demonstrated similar color pH-response of films combined with anthocyanin-rich natural extract (Kaewprachu et al., 2024).

Nitrogenous volatiles including ammonia, dimethylamine, and trimethylamine produced by food spoilage are hydrolyzed to produce OH^- and NH_4^+ and can raise pH value inside food packaging and alter the color of smart packaging films. Therefore, sensitivities of films to volatile basic compounds could be assessed by determination of its color ammonia-sensitivities. The ammonia sensitivity of the MES-GG and MES-GG-RNE films was evaluated by determining their color variation using the MES-GG film as color standard. As depicted in Table 3, the MES-GG-RNE-I, MES-GG-RNE-II and MES-GG-RNE-III films showed different could be detected by naked eyes. ΔL values of MES-GG and MES-GG-RNE films were reduced significantly as the time exposed in ammonia gas prolonged, indicating the film color was darkened in NH_3 gas. However, as the times exposed to NH_3 gas were prolonged, Δa values of MES-GG-RNE films were markedly reduced, while Δb values were markedly enhanced ($p < 0.05$), implying colors of the MES-GG-

Table 3
Ammonia sensitivity of the MES-GG and MES-GG-RNE films.

Film	Time (min)	ΔL	Δa	Δb	ΔE	Color
MES-GG	0	93.04	−0.33	3.98	–	
	20	−0.79 ± 0.11 [a]	−0.11 ± 0.01 [a]	−0.62 ± 0.06 [b]	1.01 ± 0.09 [a]	
	40	−0.72 ± 0.04 [a]	−0.03 ± 0.04 [b]	0.44 ± 0.07 [a]	0.85 ± 0.00 [a]	
	60	−0.59 ± 0.06 [a]	−0.04 ± 0.01 [b]	0.38 ± 0.04 [a]	0.87 ± 0.06 [a]	
MES-GG-RNE-I	0	88.29	5.47	1.22	–	
	20	−1.07 ± 0.07 [a]	−6.21 ± 0.01 [a]	−0.24 ± 0.04 [a]	5.81 ± 0.68 [c]	
	40	−6.85 ± 0.28 [b]	−9.53 ± 0.04 [b]	−1.39 ± 0.08 [b]	11.78 ± 0.25 [b]	
	60	−5.71 ± 0.02 [c]	−13.76 ± 0.02 [c]	−1.61 ± 0.04 [b]	15.03 ± 0.04 [a]	
MES-GG-RNE-II	0	85.49	9.96	−0.39	–	
	20	−1.14 ± 0.06 [a]	−3.51 ± 0.00 [a]	−0.39 ± 0.02 [a]	3.85 ± 0.16 [c]	
	40	−2.57 ± 0.14 [b]	−7.78 ± 0.18 [b]	−0.68 ± 0.03 [b]	8.40 ± 0.47 [b]	
	60	−6.65 ± 0.15 [c]	−15.67 ± 0.04 [c]	−1.14 ± 0.01 [c]	17.03 ± 0.11 [a]	
MES-GG-RNE-III	0	81.05	17.45	−2.66	–	
	20	−0.16 ± 0.05 [a]	−8.58 ± 0.33 [a]	1.01 ± 0.12 [a]	8.67 ± 0.28 [c]	
	40	−0.74 ± 0.28 [b]	−16.34 ± 0.08 [b]	1.06 ± 0.05 [a]	16.39 ± 0.08 [b]	
	60	−7.29 ± 0.11 [b]	−23.18 ± 0.01 [c]	−0.57 ± 0.01 [b]	24.31 ± 0.02 [a]	

RNE films were altered from red-blue to yellow-green. There are numerous investigations carried out about the appropriateness of various anthocyanin-rich plant extracts for using as pH-sensitive films (Ren et al., 2023; Wang, Xie, et al., 2023). In the MES-GG-RNE films, the MES-GG-RNE-III film displayed the most significant alteration of colors that could be detected by naked eyes due to its highest content of anthocyanins. The color change of MES-GG-RNE films could be due to differential protonation states of the anthocyanin under various pH environments. In an acidic condition, the flavylium cation and quinoidal blue species are the predominant species and contributes to purple and red colors, respectively. In an alkaline condition, anthocyanins emerged as a form of anionic quinone base, demonstrating a blue color. In general, incorporation of RNE endowed the MES-GG films a significant sensitivity to the ammonia gas, supporting the potential application of the MES-GG-RNE films as pH sensing indicators in detecting the quality of meat foods.

3.6. Application of the films
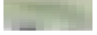
During the storage of meat products, the decomposition of proteins caused by enzymes and microorganisms can product some volatile nitrogen-based compounds such as ammonia and amines, which can be detected by pH indicator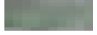 in intelligent packaging films (Jiang, Zhang, & Jiang, 2023). Due to that incorporation of RNE greatly enhanced the sensitivity of the MES-GG film to pH and ammonia gas, the three MES-GG-RNE films were used in detecting the freshness of beef meat and their potential application in monitoring the freshness degree of meat products were estimated. The TVB-N content of beef meat was gradually increased during storage at 20 °C as been depicted in Table 4. The TVB-N level was increased from 4.98 mg/100 g to 14.41 mg/100 g; meanwhile, the MES-GG-RNE films demonstrated a red color change until the storage time of 24 h (Table 4). With the RNE addition content was increased, the color of film exposed in the beef meat packaging surroundings became deepened, which was in accordance with the results of study on ammonia-sensitivity of the films. As the storage time was prolonged to 36 h, the films showed macroscopic blue dots and these dots became more with the addition amount of RNE was increased. According to the Chinese Standard GB 2707–2016, the TVB-N content to discriminate fresh and spoilage beef is 15 mg/100 g. The level of TVB-N at 36 h was 20.18 mg/100 g, which indicated the meat was spoiled and could not been consumed. At the storage time of 48 h, the MES-GG-RNE films became green. When the storage time was at 60 h, the color of films became dark green. These findings indicated that the MES-GG-RNE films could be employed as a pH-sensitive film for the freshness recognition of beef meat with the naked eyes during the packaging storage. Some researchers recently have verified the films incorporated with anthocyanins extracted from various plants could be used as indicators in monitoring the freshness of meat and aquatic foods (Ren et al., 2023). The change in color of the MES-GG-RNE-III film was more significant than the MES-GG-RNE-I and MES-GG-RNE-II films at that time. The study revealed that the films containing the anthocyanin-rich RNE solution, especially the film of MES-GG-RNE-III was suitable for discriminating the deterioration of beef products.

4. Conclusion

In this study, the pH-responsive smart composite films including MES, MES-GG and MES-GG-RNE were fabricated with MES, GG and RNE by using solution casting method. The RNE solution exhibited pH-responsiveness, showing distinct color changes in different buffer solutions. The MES-GG film showed decreased WCA and enhanced TS and EAB compared with the MES film. Incorporation with RNE could significantly decrease WVP, MC and TS of the MES-GG film. Both GG and RNE exhibited good compatibility and significantly enhanced the thermal stability and light barrier performance of the MES film. The MES-GG-RNE films showed excellent pH and ammonia response sensitivity

Table 4

Variation of the beef meat TVB-N content and MES-GG-RNE film color response to storing time.

Time (h)	TVB-N level (mg/ 100 g)	MES-GG-RNE-I	MES-GG-RNE-II	MES-GG-RNE-III
0	4.98 ± 0.25 [e]			
24	14.41 ± 0.21 [d]			
36	20.18 ± 0.77 [c]			
48	45.39 ± 0.48 [b]			
60	60.91 ± 0.75 [a]			

and dose-dependent DPPH and ABTS free radical scavenging activity. When employed for monitoring the freshness of beef meat, the MES-GG-RNE films were sensitive to the change in beef freshness. Our results suggested that the MES-GG-RNE films could be served as intelligent packaging films to monitor the freshness of animal-based protein foods.

CRediT authorship contribution statement

Changxing Jiang: Writing – review & editing, Writing – original draft, Supervision, Methodology, Investigation, Funding acquisition, Conceptualization. **Hongwu Yang:** Writing – review & editing. **Tingting Liu:** Writing – review & editing. **Qian Zhang:** Investigation. **Yufei Zou:** Investigation. **Siyu Wang:** Investigation.

Declaration of competing interest

The authors declare that there are no conflicts of interest.

Data availability

Data will be made available on request.

Acknowledgements

References

Cao, J., Wang, C., Zou, Y., Xu, Y., Wang, S., Jiang, C., Liu, T., Zhou, X., Zhang, Q., & Li, S. (2023). Colorimetric and antioxidant films based on biodegradable polymers and black nightshade (*Solanum nigrum* L.) extract for visually monitoring *Cyclina sinensis* freshness. *Food Chemistry: X, 18,* Article 100661.

Elhadef, K., Chaari, M., Akermi, S., Ben Hlima, H., Ennouri, M., Abdelkafi, S., … Smaoui, S. (2024). pH-sensitive films based on carboxymethyl cellulose/date pits anthocyanins: A convenient colorimetric indicator for beef meat freshness tracking. *Food Bioscience, 57,* Article 103508.

Gunathilake, I. A. D. S. R., & Somendrika, M. A. D. (2024). Development of a biodegradable packaging with antimicrobial properties from cassava starch by incorporating *Ocimum tenuiflorum* extract. *Food Chemistry Advances, 4,* Article 100658.

Guo, H., Yue, Z., Shao, C., Han, Y., Li, S., Miao, Z., Gao, S., Li, J., Li, Y., & Mi, L. (2024). Intelligent carboxymethyl cellulose composite films containing *Garcinia mangostana* shell anthocyanin with improved antioxidant and antibacterial properties. *International Journal of Biological Macromolecules, 263,* Article 130362.

Halász, K., & Csóka, L. (2018). Black chokeberry (*Aronia melanocarpa*) pomace extract immobilized in chitosan for colorimetric pH indicator film application. *Food Packaging and Shelf Life, 16,* 185–193.

Ji, S., Xu, T., Huang, W., Gao, S., Zhong, Y., Yang, X., Ahmed Hassan, M., & Lu, B. (2022). Atmospheric pressure plasma jet pretreatment to facilitate cassava starch modification with octenyl succinic anhydride. *Food Chemistry, 370,* Article 130922.

Jiang, C., Liu, T., Wang, S., Zou, Y., Cao, J., Wang, C., Hang, C., & Jin, L. (2023). Antioxidant and ammonia-sensitive films based on starch, κ-carrageenan and *Oxalis*

triangularis extract as visual indicator of beef meat spoilage. *International Journal of Biological Macromolecules, 235*, Article 123698.

Jiang, H., Zhang, W., Cao, J., & Jiang, W. (2023). Development of biodegradable active films based on longan seed starch incorporated with banana flower bract anthocyanin extracts and applications in food freshness indication. *International Journal of Biological Macromolecules, 251*, Article 126372.

Jiang, H., Zhang, W., & Jiang, W. (2023). Effects of purple passion fruit peel extracts on characteristics of *Pouteria campechiana* seed starch films and the application in discernible detection of shrimp freshness. *Food Hydrocolloids, 138*, Article 108477.

Jiang, L., Wang, F., Xie, X., Xie, C., Li, A., Xia, N., Gong, X., & Zhang, H. (2022). Development and characterization of chitosan/guar gum active packaging containing walnut green husk extract and its application on fresh-cut apple preservation. *International Journal of Biological Macromolecules, 209*, 1307–1318.

Kaewprachu, P., Romruen, O., Jaisan, C., Rawdkuen, S., & Klunklin, W. (2024). Smart colorimetric sensing films based on carboxymethyl cellulose incorporated with a natural pH indicator. *International Journal of Biological Macromolecules, 259*, Article 129156.

Kaith, B. S., Sharma, K., Kumar, V., Kumar, V., Swart, H. C., & Kalia, S. (2014). Effects of swift heavy ion beam irradiation on the structural and morphological properties of poly(methacrylic acid) cross-linked gum ghatti films. *Vacuum, 101*, 166–170.

Li, H., Pu, Y., Kumar, R., Ragauskas, A. J., & Wyman, C. E. (2014). Investigation of lignin deposition on cellulose during hydrothermal pretreatment, its effect on cellulose hydrolysis, and underlying mechanisms. *Biotechnology and Bioengineering, 111*, 485–492.

Li, J., Zhang, X., Lv, J., Yang, J., Liu, X., Zhang, X., & Zhang, W. (2024). Fabrication and characterization of blue honeysuckle anthocyanins-loaded nanocomposite films and the application in pork preservation. *Food Hydrocolloids, 149*, Article 109600.

Li, R., Feng, H., Wang, S., Zhuang, D., & Zhu, J. (2024). A colorimetry-enhanced tri-functional film with high stability by polyphenol-anthocyanin co-pigmentation/conjugate: New prospect for active intelligent food packaging. *Food Chemistry, 447*, Article 138927.

Liang, T., Wang, H., Shu, Y., Khan, S., Li, C., & Zhang, Z. (2024). An intelligent film based on self-assembly of funoran and *Ophiopogon japonicus* seed anthocyanins and its application in monitoring protein rich food freshness. *Food Control, 159*, Article 110300.

Liu, Q.-R., Wang, W., Qi, J., Huang, Q., & Xiao, J. (2019). Oregano essential oil loaded soybean polysaccharide films: Effect of Pickering type immobilization on physical and antimicrobial properties. *Food Hydrocolloids, 87*, 165–172.

Merz, B., Capello, C., Leandro, G. C., Moritz, D. E., Monteiro, A. R., & Valencia, G. A. (2020). A novel colorimetric indicator film based on chitosan, polyvinyl alcohol and anthocyanins from jambolan (*Syzygium cumini*) fruit for monitoring shrimp freshness. *International Journal of Biological Macromolecules, 153*, 625–632.

Mouzahim, M. E., Eddarai, E. M., Eladaoui, S., Guenbour, A., Bellaouchou, A., Zarrouk, A., & Boussen, R. (2023). Effect of kaolin clay and *Ficus carica* mediated silver nanoparticles on chitosan food packaging film for fresh apple slice preservation. *Food Chemistry, 410*, Article 135470.

Paunović, S. M., Mašković, P., Nikolić, M., & Miletić, R. (2017). Bioactive compounds and antimicrobial activity of black currant (*Ribes nigrum* L.) berries and leaves extract obtained by different soil management system. *Scientia Horticulturae, 222*, 69–75.

Prietto, L., Mirapalhete, T. C., Pinto, V. Z., Hoffmann, J. F., Vanier, N. L., Lim, L.-T., … da Rosa Zavareze, E. (2017). pH-sensitive films containing anthocyanins extracted from black bean seed coat and red cabbage. *LWT-Food Science and Technology, 80*, 492–500.

Ranjbar, M., Azizi Tabrizzad, M. H., Asadi, G., & Ahari, H. (2023). Investigating the microbial properties of sodium alginate/chitosan edible film containing red beetroot

anthocyanin extract for smart packaging in chicken fillet as a pH indicator. *Heliyon, 9*, Article e18879.

Ren, G., He, Y., Lv, J., Zhu, Y., Xue, Z., Zhan, Y., Sun, Y., Luo, X., Li, T., Song, Y., Niu, F., Huang, M., Fang, S., Fu, L., & Xie, H. (2023). Highly biologically active and pH-sensitive collagen hydrolysate-chitosan film loaded with red cabbage extracts realizing dynamic visualization and preservation of shrimp freshness. *International Journal of Biological Macromolecules, 233*, Article 123414.

Slimestad, R., & Solheim, H. (2002). Anthocyanins from black currants (*Ribes nigrum* L.). *Journal of Agricultural and Food Chemistry, 50*, 3228–3231.

Wang, C., Cao, J., Liu, T., Jin, L., Hang, C., Zhang, C., Qian, X., Jiang, D., & Jiang, C. (2023). Preparation and characterization of antioxidant and pH-sensitive films based on arrowhead (*Sagittaria sagittifolia*) starch, κ-carrageenan and black chokeberry (*Aronia melanocarpa*) extract for monitoring spoilage of chicken wings. *International Journal of Biological Macromolecules, 224*, 544–555.

Wang, F., Xie, C., Tang, H., Hao, W., Wu, J., Sun, Y., Sun, J., Liu, Y., & Jiang, L. (2023). Development, characterization and application of intelligent/active packaging of chitosan/chitin nanofibers films containing eggplant anthocyanins. *Food Hydrocolloids, 139*, Article 108496.

Wang, X., Xie, Y., Ge, H., Chen, L., Wang, J., Zhang, S., Guo, Y., Li, Z., & Feng, X. (2018). Physical properties and antioxidant capacity of chitosan/epigallocatechin-3-gallate films reinforced with nano-bacterial cellulose. *Carbohydrate Polymers, 179*, 207–220.

Wang, X., Yong, H., Gao, L., Li, L., Jin, M., & Liu, J. (2019). Preparation and characterization of antioxidant and pH-sensitive films based on chitosan and black soybean seed coat extract. *Food Hydrocolloids, 89*, 56–66.

Wang, Y., Du, H., Xie, M., Ma, G., Yang, W., Hu, Q., & Pei, F. (2019). Characterization of the physical properties and biological activity of chitosan films grafted with gallic acid and caffeic acid: A comparison study. *Food Packaging and Shelf Life, 22*, Article 100401.

Yong, H., Liu, J., Qin, Y., & Bai, R. (2019). Antioxidant and pH-sensitive films developed by incorporating purple and black rice extracts into chitosan matrix. *International Journal of Biological Macromolecules, 137*, 307–316.

Yong, H., Wang, X., Bai, R., Miao, Z., Zhang, X., & Liu, J. (2019). Development of antioxidant and intelligent pH-sensing packaging films by incorporating purple-fleshed sweet potato extract into chitosan matrix. *Food Hydrocolloids, 90*, 216–224.

Zhang, C., Chi, W., Zhou, T., Wang, Y., Li, J., & Wang, L. (2023). Fabricating a visibly colorimetric film via self-releasing of anthocyanins from distributed mulberry pomace particles in hydrophilic sodium carboxymethyl starch-based matrix to monitor meat freshness. *International Journal of Biological Macromolecules, 246*, Article 125617.

Zhang, M., Yang, B., Yuan, Z., Sheng, Q., Jin, C., Qi, J., Yu, M., Liu, Y., & Xiong, G. (2023). Preparation and performance testing of corn starch/pullulan/gallic acid multicomponent composite films for active food packaging. *Food Chemistry: X, 19*, Article 100782.

Zhang, X., Liu, J., Qian, C., Kan, J., & Jin, C. (2019). Effect of grafting method on the physical property and antioxidant potential of chitosan film functionalized with gallic acid. *Food Hydrocolloids, 89*, 1–10.

Zhang, X., Liu, Y., Yong, H., Qin, Y., Liu, J., & Liu, J. (2019). Development of multifunctional food packaging films based on chitosan, TiO₂ nanoparticles and anthocyanin-rich black plum. *Food Hydrocolloids, 94*, 80–92.

Zhao, R., Chen, J., Yu, S., Niu, R., Yang, Z., Wang, H., Cheng, H., Ye, X., Liu, D., & Wang, W. (2023). Active chitosan/gum Arabic-based emulsion films reinforced with thyme oil encapsulating blood orange anthocyanins: Improving multi-functionality. *Food Hydrocolloids, 134*, Article 108094.

Zhou, N., Wang, L., You, P., Wang, L., Mu, R., & Pang, J. (2021). Preparation of pH-sensitive food packaging film based on konjac glucomannan and hydroxypropyl methyl cellulose incorporated with mulberry extract. *International Journal of Biological Macromolecules, 172*, 515–523.